

Super-adiabatic combustion of liquid fuels through porous media

Sumrerng Jugjai* and Kittisak Suwanwijit

Combustion and Engine Research Laboratory (CERL)

Department of Mechanical Engineering, Faculty of Engineering, King Mongkut's University of Technology Thonburi
91 Prachauthit Road (Suksawad 48) Bangmod, Thung Kharu District, Bangkok 10140

Tel. 0-2470-9128, Fax. 0-2470-9111,

E-mail: sumrueng.jug@kmutt.ac.th

Abstract

A new type of high-efficiency trickling-flow liquid fuel-fired porous burner (**LFPB**) is proposed. Making use of heat re-circulated from products to the liquid fuel (kerosene) by thermal radiation emitted from porous media, both surface-stabilized and matrix-stabilized super-adiabatic combustion flames were established. The effect of the distance between porous burner (PB) and porous emitter (PE) within the LFPB, has been studied and has been found to strongly affect the combustion characteristics of the burner. The matrix-stabilized flame combustion regime has been found to produce a higher super-adiabatic temperature with relatively lower CO and NO_x concentrations. It also produces a more stable combustion region when compared with the surface-stabilized combustion flame. With the optimum inter-distance between the burner and the emitter, the LFPB system with matrix-stabilized super-adiabatic combustion yields a performance comparable with that of a well-designed conventional spray combustion system which has been equipped with exhaust gas recirculation (EGR) and staged combustion techniques. This is achieved with higher combustion intensity and at less cost. The LFPB system has the potential to replace conventional spray combustion burners in the future.

1. Introduction

Based on the previous study on the liquid fuels-fired porous burner without atomization [1] (hereafter referred to as LFPB), it appears that the inter-distance between the porous burner (PB) and the porous emitter (PE) is an important parameter in controlling combustion performance of LFPB. It can be speculated that different inter-distance between the PB and the PE could result in different combustion regime, which in turn results in different evaporation characteristics and the subsequent combustion performance. This paper studies details aspect of the inter-distance between the PB and the PE and to optimize it so as to obtain maximum possible burner performance of the LFPB.

2. State of the art technology

Heat-recirculating combustion [2] is a promising scheme to enhance combustion. Reactants are preheated

prior to the flame zone by heat transfer from burned products without mixing two streams. Fig. 1 shows comparison in temperature histories of premixed combustion in a one-dimensional adiabatic system for the cases with and without heat-recirculation. There is no ceiling on the maximum combustion temperature for the case with the heat-recirculation depending on the amount of heat recycled. However, unlimited amount of the recycled heat is not desirable in practical applications because of limitation of the maximum working temperature of material, high emission of oxide of nitrogen (NO_x) and undesirable risk of pre-ignition of the mixture. Therefore optimization of temperature, combustion efficiency and emission of pollutants are important. This combustion is sometimes referred to in terms of its "excess enthalpies" or "super-adiabatic flame temperature" for reason obvious on inspection of Fig. 1, and it is interesting to extend this to burn liquid fuel.

3. Experiment

Fig. 2 shows details of the LFPB. It comprises a porous burner (PB) and a porous emitter (PE) with a swirl chamber separating them. The liquid kerosene is supplied through the PB at its upstream end with a trickling flow by a syringe, whereas the fuel vapor leaves the downstream end and immediately mixes with the combustion air in the swirl chamber. Combustion occurs either in the swirl chamber or within the PE or both depending on operating conditions. Heat is recirculated to the PB by thermal radiation emitted from flame or the PE for evaporation within the PB. Main components of the apparatus, dimensions, operating procedure and measuring devices for temperatures T , concentration of CO and NO_x, combustion pressure ΔP , flow rate of the liquid fuel (kerosene) and flow rate of the combustion air remain the same as was used in the previous work [1]. However, three major modifications have been made in the present study: (1) independent axial movement of the PE and PB are provided, allowing for adjustment in the inter-distance between PB and PE or volume of the swirl chamber. This inter-distance can be represented by the summation of absolute values of x_{PE} and x_{PB} , which is, respectively,

* Corresponding author

represents the position of the upstream surface of PE and the position of the downstream surface of PB with respect to the reference position at the exit of the swirling air ($x = 0$). Variation in x_{PE} and x_{PB} could be independently achieved by turning axial screws (not shown) mounted at the free ends of PE and PB. (2) installation of a rotating axle (not shown) perpendicular to the center line of the burner is done so as to allow for variation in the burner angle θ , and (3) relocation of the fuel injector (syringe) with its tip making direct contact with the upstream end of the PB is conducted. This is to eliminate the dead space just above the PB as is designed in the previous work [1], thus preventing the liquid fuel stream from impinging on the side wall and avoiding accumulation of the liquid fuel within the space.

The LFPB, at a down-flow combustion ($\theta = 0^\circ$), was started first by preheating the burner with turbulent diffusion flame obtained by supplying liquefied petroleum gas (LPG) through the PB before switching to liquid kerosene when the temperature at the downstream region of the PB T_6 attained a favorable value for continuous evaporation (500-800 °C) and auto-ignition. Under normal operating conditions, only liquid fuel was supplied through the PB and reacts with the swirling air downstream. T , ΔP and concentration of CO and NO_x were recorded as a steady state condition was reached. Focus has been made on studying effect of x_{PE} and x_{PB} at various burner angle θ on combustion regime, temperature profiles and emission characteristics.

4. Results and discussion

4.1 Surface-stabilized flame

An experiment on combustion of liquid kerosene by the porous burner PB ($\tau_{PB} = 131$) without PE ($\tau_{PE} = 0$) is carried out first to show a high potential of the LFPB in rendering a surface-stabilized flame of liquid fuel without atomization. Here τ is an optical thickness, which is a measure of the ability of a medium to attenuate energy and is equal to the extinction coefficient (having unit in length^{-1}) integrated over the path length.

Fig. 3 shows an effect of x_{PB} on T at various θ of the surface-stabilized flame. Variation in X_{PB} was done within a limited range of about $-40\text{ mm} \leq X_{PB} \leq -5\text{ mm}$. Out of this range, no experiment was conducted because of appearance of soot if X_{PB} being less than -40 mm and blockage of the swirling air if X_{PB} was larger than -5 mm (see Fig. 2). Effect of x_{PB} on T is strongly dependent on θ . At $\theta = 0^\circ$ the zone of chemical reaction is confined and peaked near exit of the swirling air irrespective of x_{PB} . On the other hand, at $\theta = 90^\circ$ and $\theta = 180^\circ$, x_{PB} strongly affects T yielding a long radius curvature temperature profiles without a peak value. This implies lengthening of the combustion zone, which is attributable to buoyancy effect especially when $\theta = 180^\circ$. In every case, a combustion regime of surface-stabilized flame that occurs near the downstream end of the PB was achieved. Moreover, at

some specified value of x_{PB} , a peak of non-equilibrium temperature that slightly exceeds the adiabatic flame temperature of usual (without porous medium) liquid flames, T_{ad} , was observed. This is because some heat of combustion of the products is internally transferred by flame radiation through a solid matrix of the PB for preheating and evaporating the liquid fuel. Because of inter-phase thermal non-equilibrium within the PB, the fuel vapor, before mixing and ignition, is additionally heated which results in super-adiabatic combustion and the formation of the peak of super-adiabatic temperature as observed, though slightly.

Fig. 4 confirmed an independence of location of the reaction zone (specified by location of the maximum temperature, $X_{T_{max}}$) on X_{PB} and was fixed at $X_{T_{max}} = 5$ mm for $\theta = 0^\circ$. The maximum temperature was almost constant before showing a decreasing trend as the surface of the PB is exactly at the same location of the exit of the swirling air ($X_{PB} = -5\text{ mm}$). The independence of $X_{T_{max}}$ on X_{PB} is beneficial to not only an evaporation of liquid fuel within the PB but also a favorable mixing process between fuel vapor emerging from the PB and the swirling air in the swirl chamber. Enhanced evaporation followed by a more homogeneous combustion could be achieved with minimum CO and NO_x emission among the three burner angle as shown in Fig. 5. Moreover, CO is almost independent of X_{PB} , whereas NO_x shows a slight increase with X_{PB} .

In contrast at $\theta = 180^\circ$ (Fig. 4), $X_{T_{max}}$ was constant at $X_{T_{max}} = 55$ mm and is irrespective the value of X_{PB} only when $-40 \leq X_{PB} \leq -30$ before showing an increasing trend with X_{PB} . Moreover, emissions of CO and NO_x are maximum among the three burner angles θ as shown in Fig. 5, particularly for CO emission within the range of $-15\text{ mm} \leq X_{PB} \leq -5\text{ mm}$ due to a strong quenching effect. An increase in NO_x may be attributable to prolong of the residence time within the high temperature zone caused by a relatively long curvature of the temperature profile as shown in Fig. 3 ($\theta = 180^\circ$). $\theta = 90^\circ$ yields an intermediate effect of X_{PB} between $\theta = 0^\circ$ and $\theta = 180^\circ$. Based on the minimum in CO emission as shown in Fig. 5, $X_{PB} = -10$ mm is suitable for $\theta = 0^\circ$, whereas $X_{PB} = -35$ mm is suitable for $\theta = 90^\circ$ and $\theta = 180^\circ$.

4.2 Matrix-stabilized flame ($\theta = 0^\circ$)

With PE ($\tau_{PE} = 2.8$) installed, T_{max} occurred within the PE implying a matrix-stabilized flame as shown in

Fig. 6 ($\theta = 0^\circ$). Moreover, the super-adiabatic combustion regime becomes prominent with T_{\max} exceeding T_{ad} and T_{\max} of the surface-stabilized flame. X_{PE} strongly affects T . The smaller the value of X_{PE} is, the deeper the flame location stabilized within the PE. Increase in CL will further push the flame deeper within the PE as shown in Fig. 7. This can be understood by observing the sign of the quantity $(X_{T_{\max}} - X_{PE})$. Minus sign implies a surface-stabilized flame near the surface of the PB, whereas a positive one implies a matrix-stabilized flame. $(X_{T_{\max}} - X_{PE}) = 0$ means a partially matrix-stabilized flame with flame stabilized at the inlet of the PE. An interesting feature is a simultaneous decrease in CO and NO_x with a decrease in x_{PE} . These emissions are smaller than those of the surface-stabilized flame at the same experimental condition as shown in Fig. 8. Moreover, if the inter-distance between PB and PE was decreased to 10 mm, which is the smallest value that could be achieved with $X_{PB} = -5$ mm, $X_{PE} = 5$ mm or equivalent to the exit diameter of the swirling air, a deeper flame location within the PE (Fig. 7) with higher T_{\max} (Fig. 6) and almost constant CO and NO_x (Fig. 8) as compared with the case for $X_{PB} = -15$ mm, $X_{PE} = 5$ mm was achieved at the same CL = 6.65 kW. However, the combustion can not be considered as an absolute matrix-stabilized flame unless the swirl chamber is removed.

To prove this hypothesis, a double layer of PE comprising two different diameter of ceramic spheres with $d_p = 7$ mm and $d_p = 19$ mm was used instead of a single layer one with constant $d_p = 19$ mm. The upstream section of a double layer PE was formed by ceramic spheres of $d_p = 7$ mm with 50 mm long, whereas the downstream one consists of $d_p = 19$ mm spheres. This arrangement can help to avoid blockage of the swirling air that may be caused by a relatively larger diameter sphere as compared with exit diameter of the swirling air (10 mm).

Fig. 10 shows flat temperature profile (with its value lower than T_{boil}) covering the PB and the upstream portion of in PE up to or slightly beyond exit of the swirling air followed by an abrupt increase in the temperature somewhere downstream due to combustion. Location of the combustion zone strongly depends on CL. Although stable combustion was achieved, only a narrow range of CL could be adjusted at typical constant equivalence ratio $\Phi = 0.8$ with relatively large emission of CO as compared with the system with the swirl chamber as shown in Fig. 11. Unlike the system with the swirl chamber, the system without the swirl chamber, however, has shown no separate and independent phenomena; i.e. a complete evaporation within the PE and a combustion at the immediate or slightly downstream the exit of the swirling air. The system without the swirl chamber yields evaporation, mixing and combustion phenomena simultaneously taking place at or slightly downstream of the exit of the swirling air depending on experimental conditions. Filling up the swirl chamber with ceramic

spheres may significantly reduce energy recirculation by thermal radiation to the PB owing to thermal radiation blockage caused by increase in the opacity of the swirl chamber. Evaporation rate within the PB may significantly be reduced. Mixing process between fuel vapor and combustion air may be poor due to blockage of the ceramic spheres, leading to a more heterogeneous combustion. An imbalance between rate of evaporation and rate of combustion becomes critical, eventually resulting in a narrowing in the stable combustion range.

Swirl chamber is important and necessary for stable and complete combustion. With optimized x_{PE} , this can lead to maximum net radiative heat flux $q^n(\tau_{PB})$ recycled to the PE as shown in Fig. 12.

$q^n(\tau_{PB})$ was calculated from the measured temperature profiles. $q^n(\tau_{PB})$ is strongly dependent on x_{PE} and it becomes maximum at optimized $x_{PE} = 10$ mm as shown in (Fig. 7). Apparently, the net radiative heat transfer $Q^n(\tau_{PB})$ is five times larger than latent heat of evaporation Q_L of the liquid kerosene. $x_{PE} = 10$ -15 mm is found to be optimal. Even smaller value than $x_{PE} = 5$ mm are also possible based on minimum CO and NO_x emission as shown in Fig. 8. Matrix-stabilized flame within PE is important, whilst its flame location has to be as close as possible to the PE inlet with minimum CO and NO_x emission. Thus, $x_{PB} = -15$ mm and $x_{PE} = 5$ mm are considered to be optimum values.

4.3 Performance of LFPB

Fig. 13 shows comparison of NO_x between the system of LFPB and the conventional spray combustion equipped with exhaust gas recirculation, EGR and staged combustion technique. Despite a non spray and non-assist with EGR and staged combustion technique, the LFPB system yields comparable NO_x emission at higher combustion density with smaller size, simpler structure and lower in cost.

5. Conclusions

Operating of LFPB with surface-stabilized flame combustion regime with optimum $|X_{PB}| = 15$ mm offers favorable wide stable combustion region irrespective of the burner angle θ . Operating the LFPB with a matrix-stabilized flame combustion regime with optimum $x_{PE} = 5$ mm yields a more prominent super-adiabatic combustion characteristic and further reduction in CO and NO_x emission and a wider stable combustion region as compared with the surface-stabilized flame.

References

- [1] S. Jugjai, N. Polmart, Exp. Therm. Fluid Sci. 27 (8) (2003) 901 - 909.
- [2] Weinberg, F.J., Ed. (1986) "Advanced Combustion Methods" Academic Press, London.
- [3] R. Villasenor, R. Escalera, Int. J. Heat Mass Transfer 41 (20) (1998) 3087-3097.

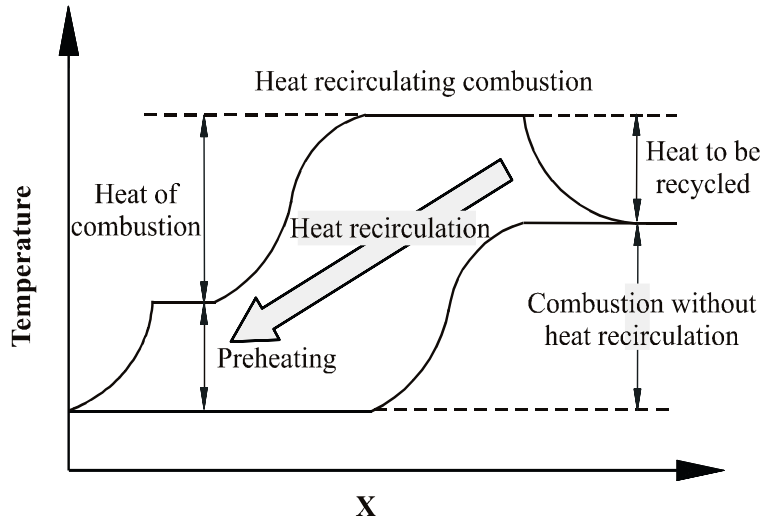


Fig. 1. Principle of heat recirculating combustion.

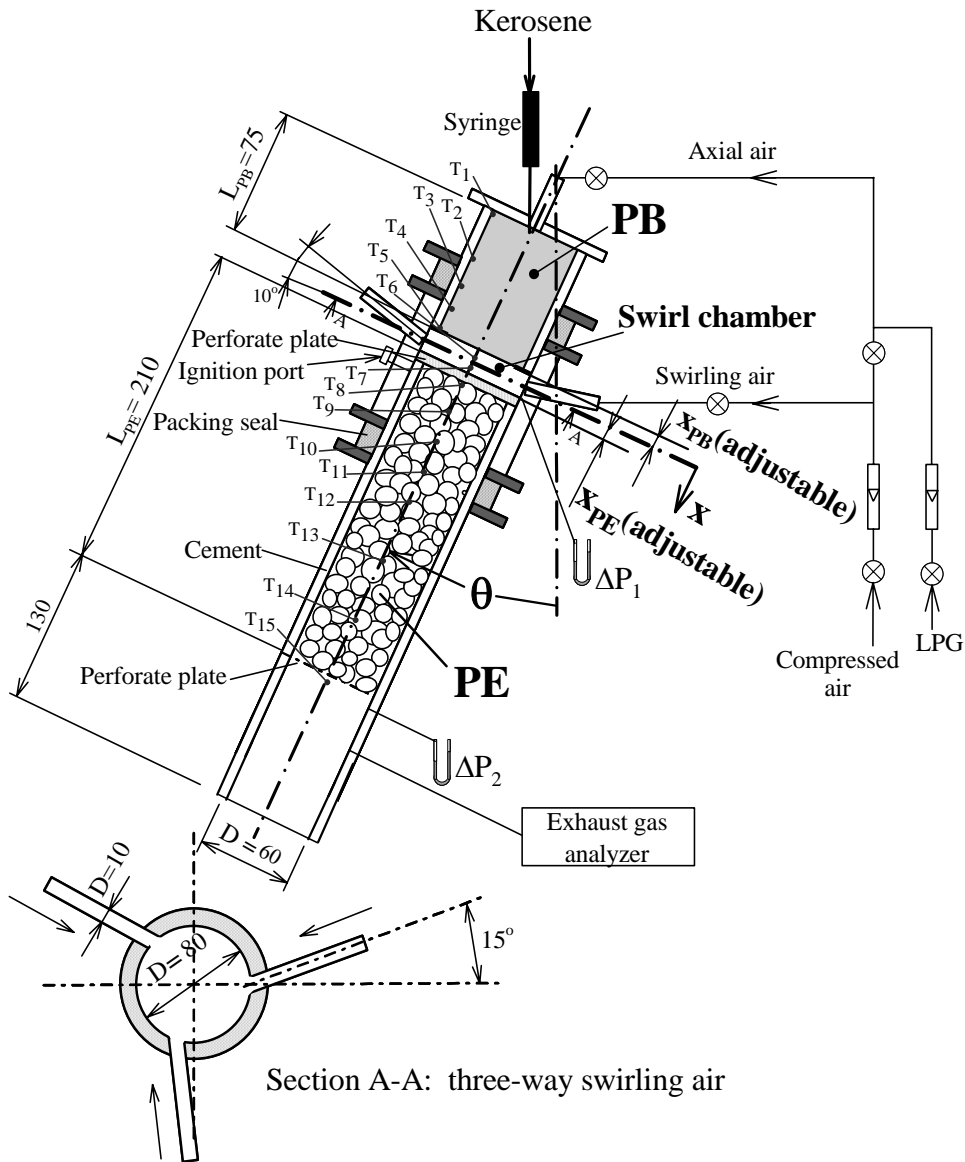


Fig. 2. Details of LFPB.

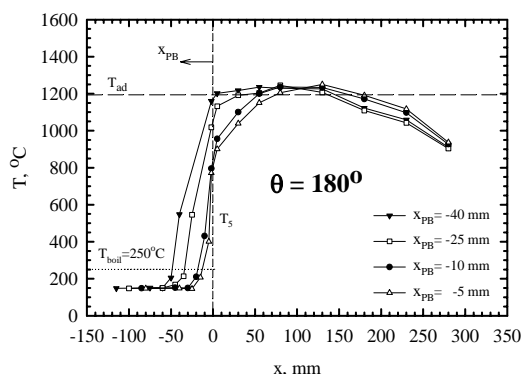
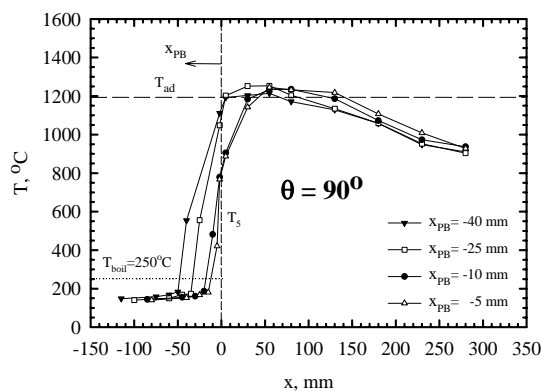
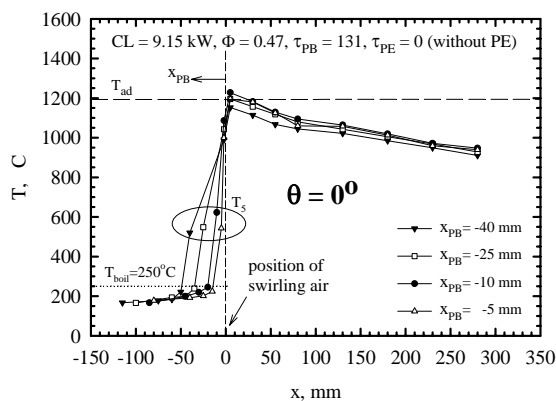


Fig. 3 Effect of x_{PB} on T at various θ of surface-stabilized flame.

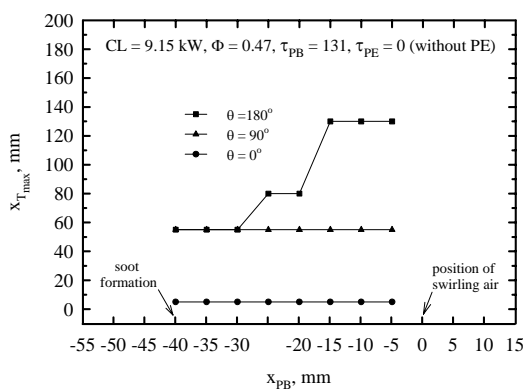


Fig. 4. Effect of x_{PB} on x_{Tmax} at various θ of surface-stabilized flame.

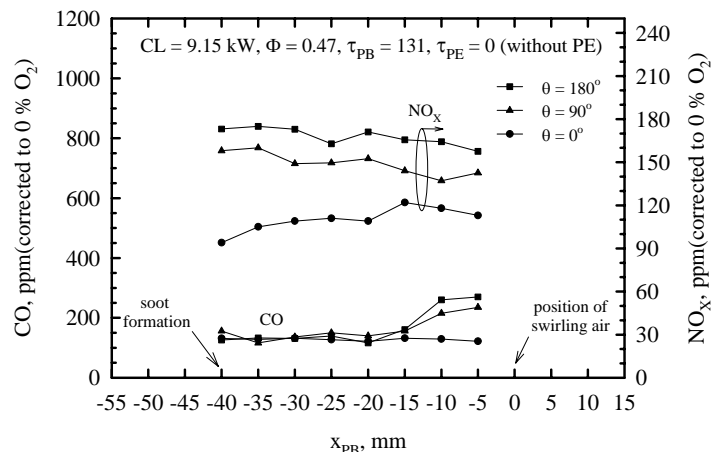


Fig. 5. Effect of x_{PB} on CO and NO_x at various θ of surface-stabilized flame.

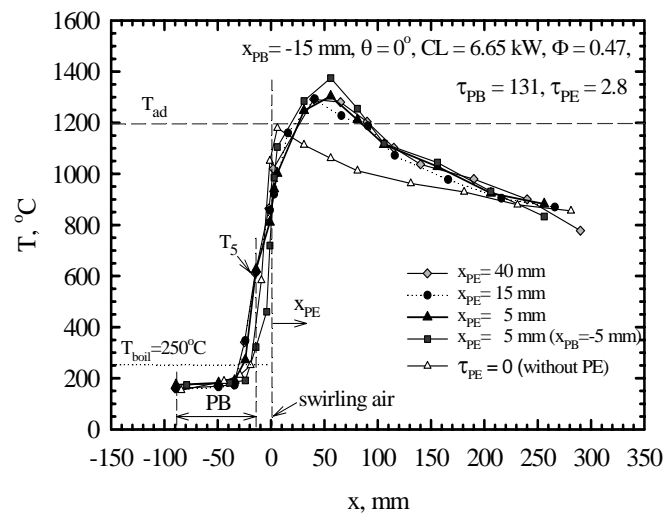


Fig. 6. Effect of PE and x_{PE} on T at $\theta = 0^\circ$ of matrix-stabilized flame.

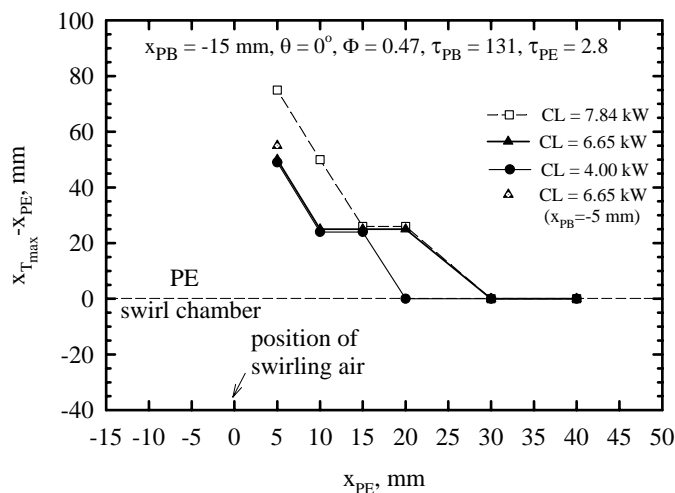


Fig. 7. Effect of x_{PE} on x_{Tmax} at $\theta = 0^\circ$ of matrix-stabilized flame.

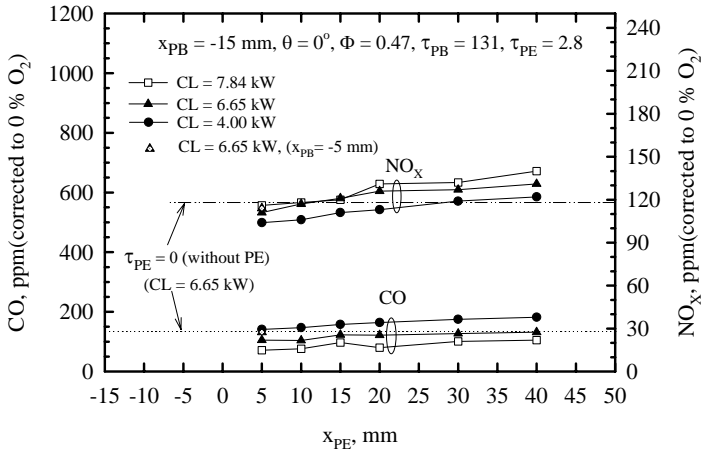


Fig. 8. Effect of x_{PE} on CO and NO_x at $\theta = 0^\circ$ of matrix-stabilized flame.

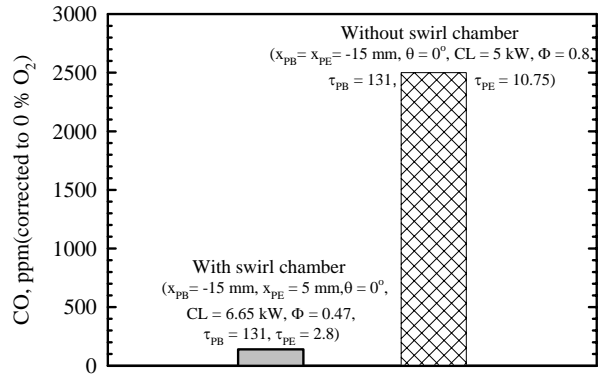


Fig. 11. Comparison in CO between with and without swirl chamber of matrix-stabilized flame.

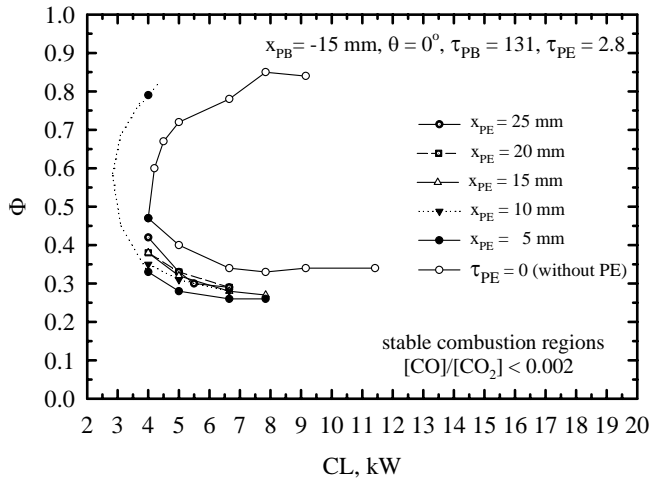


Fig. 9. Effect of PE and x_{PE} on stable combustion region at $\theta = 0^\circ$ of matrix-stabilized flame.

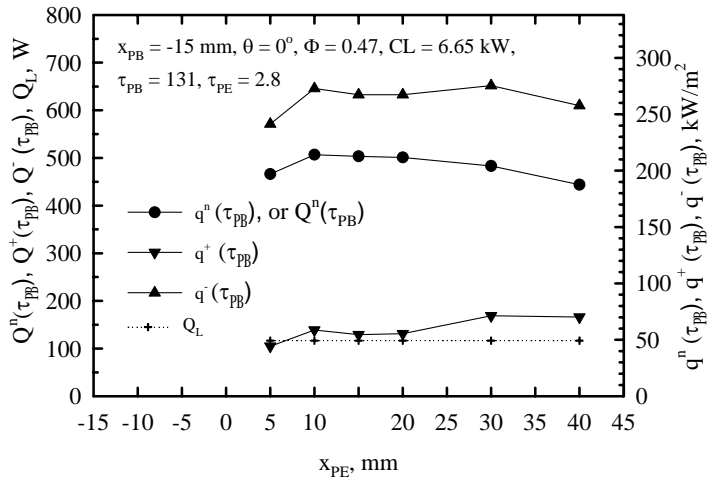


Fig. 12. Effect of x_{PE} on radiative heat fluxes in matrix-stabilized flame.

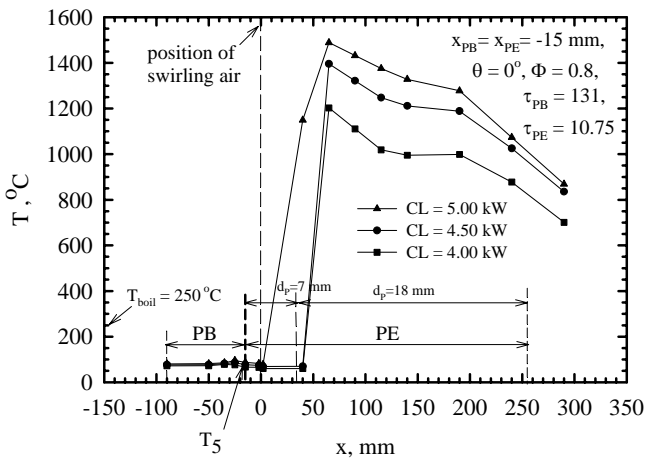


Fig. 10. Typical distribution of T at $\theta = 0^\circ$ of matrix-stabilized flame. (without swirl chamber).

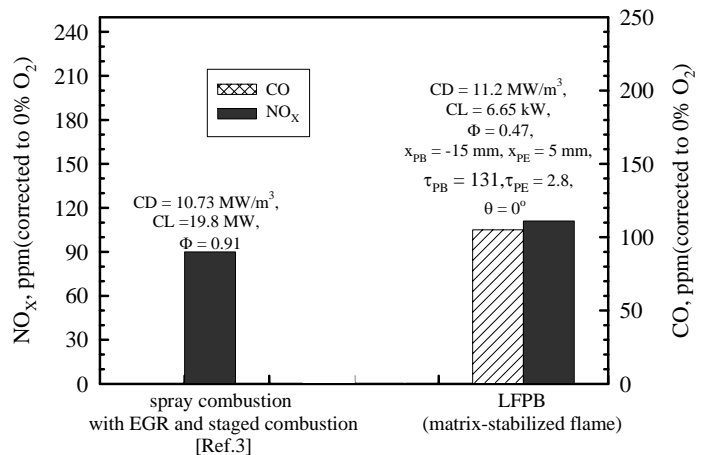


Fig. 13. Comparison in CO and NO_x between LFPB and spray combustion.